SiO_x/C Composite Anode of Lithium-Ion Batteries with Enhanced Performances Using Multicomponent Binders

Haoyuan Liu, Encheng Huangzhang, Chenhao Sun, Yanchao Fan, Zhen Ma,* Xiaoyang Zhao, and Junmin Nan*

ACCESS | 📊 Metrics & More | 📰 Article Recommendations | 🔵SI Supporting Information

ABSTRACT: A silicon suboxide−carbon (SiO_x/C, $1 \leq x \leq 2$) composite anode of lithium-ion batteries (LIBs) with enhanced performance is prepared using an aqueous multicomponent binder technology. Considering the adhesive force, electrolyte absorption, and stability, different binders including sodium alginate (SA), polyacrylamide gel (PAM), polytetrafluoroethylene (PTFE), and their composites are evaluated. It is indicated that compared to other anodes with single- or multicomponent binders, the SiO_x/C composite anode with PAM/SA/PTFE663 (PSAP663) binders exhibits strong adhesion, moderate electrolyte absorption ability, and a specific capacity of 427 mA h g^{-1} charge−discharged at 0.5 A g^{-1} after 300 cycles. The improvement of electrochemical performance is attributed to the comprehensive effects of composite binders, including the adhesion of active substances, surface protection, solution adsorption, conductive path, and so on. These results show that the PSAP663 binder has promising potential for application, which not only gives alternative practical schemes of the green binders for the SiO_x/C anodes but also provides ideas to develop a high-performance adhesive technology for LIBs.
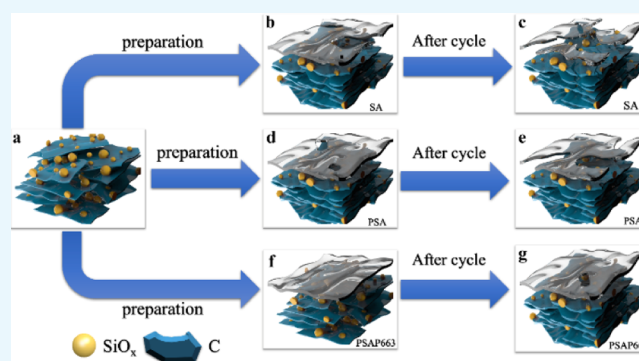
1. INTRODUCTION

With the widespread application and popularity of hybrid vehicles and portable electronic devices, low-cost and high-performance lithium-ion batteries (LIBs) have attracted much attention.[1] Compared to commercial graphite anode materials,[2−5] silicon (Si), Si-based suboxides (SiO_x, $1 \leq x \leq 2$), and their composites exhibit higher theoretical specific capacity, little difference in working potential ($\leq$0.5 V vs Li/Li$^+$), and are quite rich in resources.[6−12] However, the Si-based anode materials generally reveal low Coulombic efficiency, large volume expansion and contraction (>300%), and poor conductivity, which are also major reasons that affect the commercial application.[13−16] Besides the strategies of nano-sized and functional electrolytes, it has demonstrated that the functionalized binders can stabilize the performances of LIBs with Si-based anode materials.[17] It is still a challenge to develop the binder technology to enhance the performances of Si-based LIBs.

According to the properties of Si-based materials, it is concluded that the binders used in Si-based anodes should preferably have the following characteristics. There is an appropriate elastic capacity to adapt large volume changes; the functional groups can be used to interact with the hydroxyl groups on the Si surface to increase the bonding ability.[18−21] Thus, the hydrophilic binders with functional groups such as

hydroxyl (−OH), amino (−NH_2), carboxyl (−COOH), ester (−COO), and so forth will be considered as promising candidates.[22] Those polar functional groups of binders also contribute to the electrolyte absorption, which can make ion migration happen quickly and improve the rate performance of LIBs. The plate with excellent bonding strength ensures that the active material will not fall off the current collector after repeated expansion and contraction of the electrode, which is also a prerequisite to ensure the performances of LIBs. Since binders will be soaked in the electrolyte during the lifespan of LIBs, the binders must have excellent chemical stability and antielectrochemical reactions.[23] Also, considering the problems of practical application, the binders must also be green, pollution-free, safe, and low in price.[24]

According to the previous reports, sodium alginate (SA) has a good effect in limiting the expansion of Si-based particles. It has been gradually used in the anode of LIBs. Hu et al. used lithified polyacrylic acid (Li_xPAA) to fill the pores of the SA
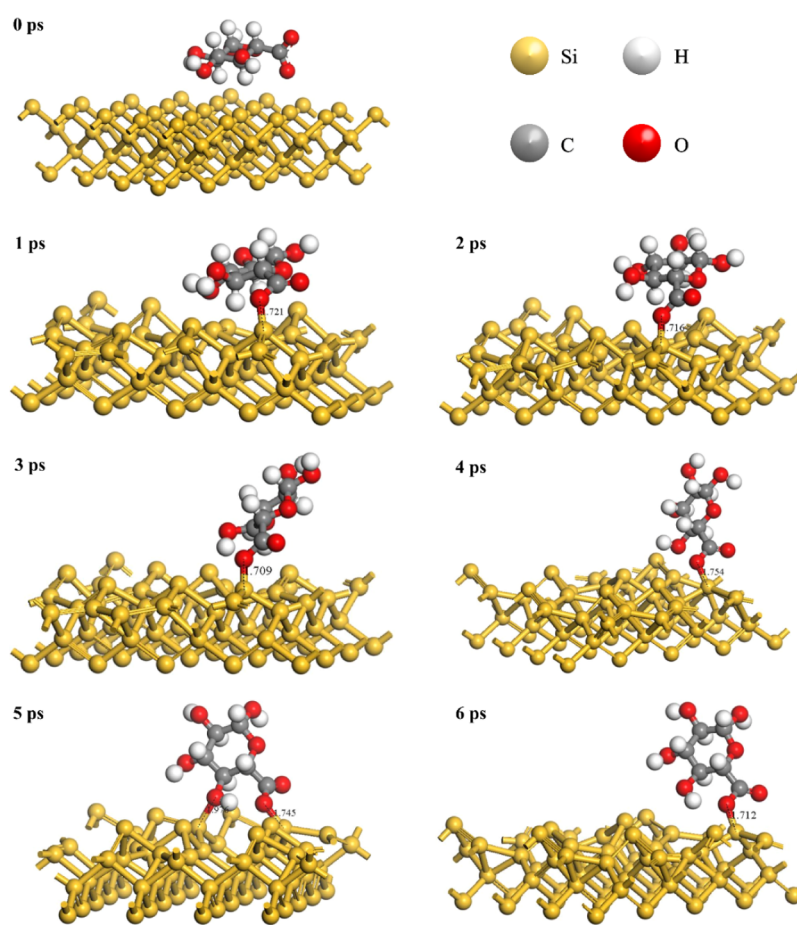
Figure 1. Snapshots for the AIMD trajectory. In these, 0−6 ps represents the bonding process between alginate anions and SiO$_x$ molecules.

network to form a cross-linked double-composite network binder (b-Li0.5PAA@SA); the volume change of Si particles (M-Si) could be effectively buffered through the extensive interlocking of interfacial ester bonds during the repeated cycle.[25] Based on the excellent electrochemical stability and corrosion resistance of polytetrafluoroethylene (PTFE) water emulsion binders, Kang et al. prepared a three-dimensional SiO$_x$ anode with good electrochemical performance by using CMC/SBR/PTFE binders.[26] In addition, it was indicated that polyacrylamide (PAM) binders could exhibit strong adhesion in the electrode and resist the penetration of organic electrolytes. The ions and covalent cross-links in the PAM binder maintained their inherent good adhesion properties and further enhanced the diffusion of lithium ions. Gendensuren et al. improved the electrochemical performance of the adhesive by introducing double-cross-linked alginate and PAM to enhance the cycling stability of SiO$_x$/C anodes.[27,28] Although the existing aqueous binder systems have revealed their advantages to improve the performances of Si-based anodes, from the perspective of commercial application, it is still necessary to further optimize the composition and performance of the aqueous binders. A good binder requires not only rigidity but also the ability to absorb the electrolyte. This is difficult to achieve using a single binder, so it needs to be achieved through the multiple binder strategy.

The above analysis can provide a good idea for the design and optimization of aqueous additive systems, which can be used to replace the conventional polyvinylidene fluoride (PVDF) binder by the green and functionalized aqueous binders. In this work, SA, PAM gel, and PTFE emulsion have been used to prepare commercial SiO$_x$−carbon (SiO$_x$/C) composite anodes with enhanced performances. It is demonstrated that the SA can connect SiO$_x$/C particles tightly through chemical bonds, facilitate the formation of a solid−electrolyte interface (SEI) film, and inhibit the decomposition of the electrolyte.[29] The PAM with rich amide functional groups not only improves the strain resistance of the plate but also increases the affinity between SiO$_x$ and other components.[30] The PTFE can form an elastic network in the electrode matrix.[31−33] These results not only give alternative practical scheme of the green binders for the SiO$_x$/C anodes but also provide ideas for the further development of high-performance adhesive technology of Si-based LIBs.

2. RESULTS AND DISCUSSION

2.1. Design and Characterization of the SiO$_x$/C Anode with a SA Binder. Figure 1 shows the quantification calculation process of the Si atom by SA. At 0 ps, the alginate anions were laid flat above the Si surface. At 1 ps after the start of molecular dynamics, the carboxylic oxygen atoms of alginate anions stripped of protons directly bonded with Si atoms. The bond length of the oxygen atom and Si of carboxyl group was 1.721 Å, and the bond angle was 126.654°. From the point of view of bond length data, it was regarded as chemical adsorption. During the process, at 2−4 ps, the alginate anion began to move in the vertical direction due to the increasing bond force (the bond length increased from 1.716 to 1.754 Å). At 5 ps, the hydrogen bonding force between the alginate
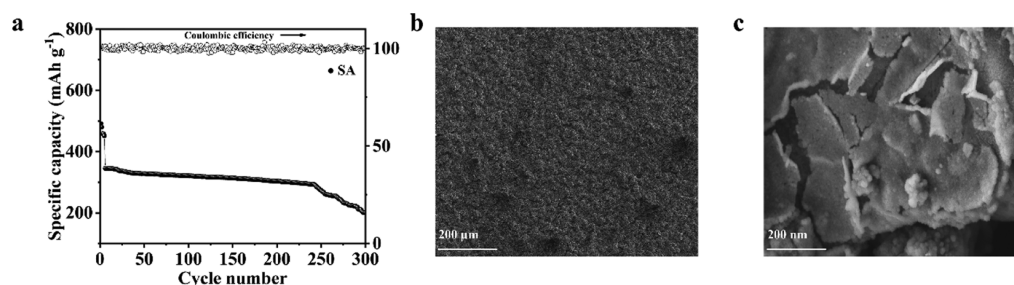
Figure 2. (a) Cycle stability and Coulombic efficiency of the SiO$_x$/C anodes with SA binders at 0.5 A g^{-1}. (b,c) SEM images of the SiO$_x$/C electrode using SA as a binder after 300 cycles.
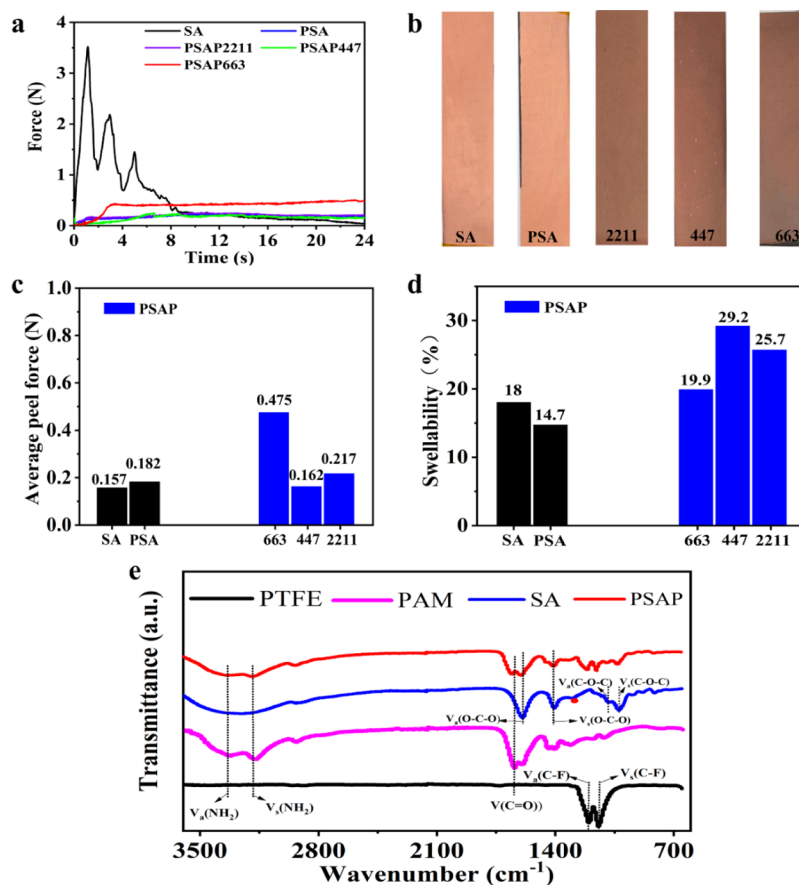
Figure 3. (a) Tension and time curves of SiO$_x$/C anodes with different binders and different PSAP ratios at 100 mm min^{-1} stripping speed. (b) Digital photos of the SiO$_x$/C anodes with different binders after the stripping test. (c,d) Average tensile parameters and swelling of the SiO$_x$/C anodes with different binders and PSAP ratios. (e) Infrared spectroscopy comparison of PTFE, PAM, SA, and PSAP in the SiO$_x$/C anode.

anion and Si atom reached the maximum value. A hydroxyl oxygen atom adjacent to the carboxyl group also formed a bond with the Si atom. The hydrogen atoms faced away from the surface, while the oxygen atoms in the carboxyl group formed bonds with Si atoms that were 1.745 Å long. Another Si−oxygen bond was 1.936 Å long. At 6 ps, because the expansion force of Si particles gradually increased as the reaction went on, the adjacent hydroxyl group bound to Si atoms became unsteady (the bond length of the carboxyl oxygen atom and Si becomes 1.712 Å), which exceeded the binding on the Si atom. Hence, the alginate anion began to slowly return to its original position. It can be seen that the surface of SiO$_x$/C was reconstructed, and the surface reconstruction was beneficial to reduce the surface energy of SiO$_x$/C. Therefore, the intermolecular interaction between

alginate anions and SiO$_x$ had a strong binding energy. In the end, the reasons for choosing SA as a base binder are discussed.

The electrochemical performance of the SiO$_x$/C electrode using SA as a binder was analyzed. Figure 2a shows that the SiO$_x$/C shows good stability in the 300 cycles, which may be due to the strong bonds formed between the ordered carboxyl functional groups inside SA and the Si atom. It was noteworthy that the charge-specific capacity in the first five cycles was greatly attenuated, which was associated with the huge physical stress caused by the repeated expansion effect of SiO$_x$ particles. Although the SA has abundant hydroxyl and carboxyl groups, the strength of the bonds formed between the SA and Si atom is not enough to maintain the structural stability under the condition of huge volume expansion caused by the insertion/
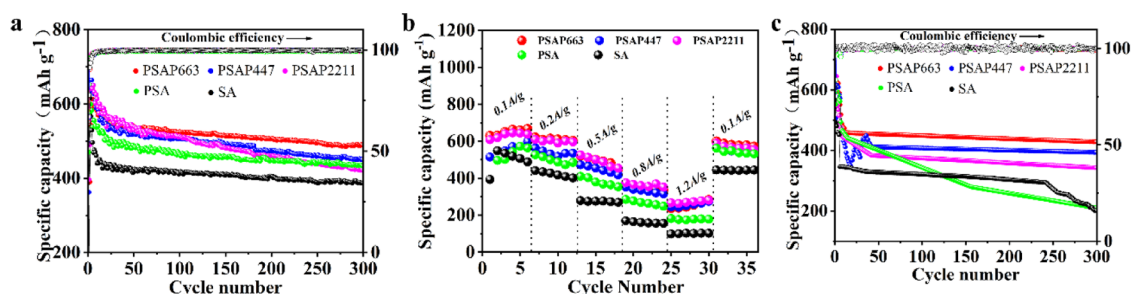
Figure 4. (a) Cycle stability and Coulombic efficiency of the SiO_x/C anodes with different binders at 0.2 A g^{-1}. (b) SiO_x/C electrode rate performance graph using the PSAP663, PSAP447, PSAP2211, PSA, and SA binders. (c) Cyclic performance and Coulombic efficiency diagrams of the SiO_x/C electrodes using PSAP663, PSAP447, PSAP2211, PSA, and SA as binders at 0.5 A g^{-1}.

deinsertion of lithium ions in SiO_x (Figure 2b,c). Therefore, more functional components need to be introduced to improve SA.

2.2. Characterization of the SiO_x/C Anodes with Different Binders. The bonding strength of different binders and the capacity of electrolyte adsorption of the SiO_x/C anodes were first evaluated. The bonding strength can reflect not only the ability to connect the active material and the collector to each other but also the limiting force to the repeated expansion of SiO_x/C particles. The capacity of electrolyte absorption is closely related to the speed of lithium-ion intercalation/deintercalation reaction and the cycling lifetime of the SiO_x/C anodes.

Table S1 shows the ratio of different binders. Figure 3a shows that the tension and time curve can be clearly obtained; the average tensile value of PSAP663 under the action of 100 mm/min is much higher than that of SiO_x/C electrode pieces with other binders. As can be seen from left to right in Figure 3b, after peeling the same distance at the same peeling speed, the amount of active material residues on PSAP663 is the largest, which indicates that the bond strength of the binder is the largest among all materials. As can be seen in Table S2 and Figure 3c, the average tensile force of PSAP663 is 0.475 N. The average tensile strength is also the largest one among all the binders, which corresponds to the result shown in Figure 3b. By color contrast, it is clear to the naked eye that the most active substance remained on PSAP663. Figure 3a−c shows that PSAP663 performs well in terms of physical viscosity, which ensures that the active material can be stably bonded with the collector and prevents the occurrence of material depowdering.

Figure 3d shows the swelling rate test chart of different water system binders soaked in the same electrolyte. On the one hand, it was to test the comparison of absorptive capacity of different binders to the electrolyte. On the other hand, it was to show that absorptive capacity of the electrolyte was also an important factor affecting adhesion. Excessive electrolyte absorption will affect the bonding effect of the binder on the material and directly affect the connection effect of the SiO_x/C material and the conductive agent. Too little liquid absorption will result in incomplete performance of the host. As shown in Figure 3d, the swelling rate of a single SA binder was 18% after soaking in the electrolyte for 12 h. The PSA absorbed less electrolyte than SA, and the PSAP663, PSAP447, and PSAP2211 absorbed more electrolyte than SA. It is noteworthy that the electrolyte absorption capacities of PSAP2211 and PSAP447 were much higher than that of SA, which may greatly affect the bonding of the two electrodes and then reduce the

stability of the electrochemical performance. Through the test of bond strength and electrolyte absorption ability, it can be preliminarily concluded that PSAP663 can effectively inhibit the volume expansion of SiO_x/C particles. Although SA can form a strong bond force with the Si atom, it did not have good rigidity and had insufficient electrolyte absorption capacity. The PAM with rich amide functional groups can improve the strain resistance of the coating layer. The PTFE can form an elastic network in the electrode matrix, and its strong electrolyte absorption capacity can ensure the transmission channel of lithium ions. Therefore, the addition of PAM and PTFE can make up for the deficiency of SA. In order to further verify the effect of the binder on the electrochemical properties of SiO_x/C materials, other properties needed to be further tested.

As can be seen in Figure 3e showing the Fourier transform infrared (FTIR) spectrum, the characteristic peak of PAM appears at 3182 and 3338 cm^{-1}, which was caused by the symmetric and asymmetric stretching vibrations of the polar functional group $-NH_2$ with rigidity, respectively, while the peak at 1645 cm^{-1} corresponds to the vibration of $-C≡O$.[34,35] For the FTIR spectrum of SA, there was a wide peak caused by asymmetric stretching vibration at 1598 cm^{-1} and a narrow peak caused by symmetrical stretching vibration at 1410 cm^{-1}, both of which were caused by the O−C−O (carboxylate) stretching vibration. A wider absorption peak at 1030 cm^{-1} is due to the C−C−H (and O−C−H) deformation of the pyranose ring and the asymmetric movement of C−O−C.[36,37] The characteristic peaks of PTFE appear at 1150 and 1206 cm^{-1}, mainly due to the symmetric and asymmetric stretching motion of $-CF$.[38] From the FTIR spectrum of PSAP, it can be seen that the characteristic absorption peaks of PAM, SA, and PTFE all appear well in PSAP, indicating that the structure and functional groups of these single binders were well retained in PSAP. However, there was a slight deviation in the position of some peaks and the peak height was reduced, which indicated that the hydroxyl aldehyde condensation reaction of functional groups such as $-COOH$, $-NH_2$, and $-C≡O$ forms a macromolecular chain, which was conducive to the closer connection between binders and the protection of the SiO_x/C electrode. Furthermore, as shown in Figure S1a, it can be concluded from these peaks of XRD spectra that crystalline Si nanoparticles were successfully bonded to graphite materials. Also, in Raman spectra (Figure S1b), the intensity of the D band is similar to that of the G band (I_D/I_G = 1.101), indicating that the crystallinity of carbon is good.

2.3. Electrochemical Performances. In order to check the effect of the multicomponent binder, a series of
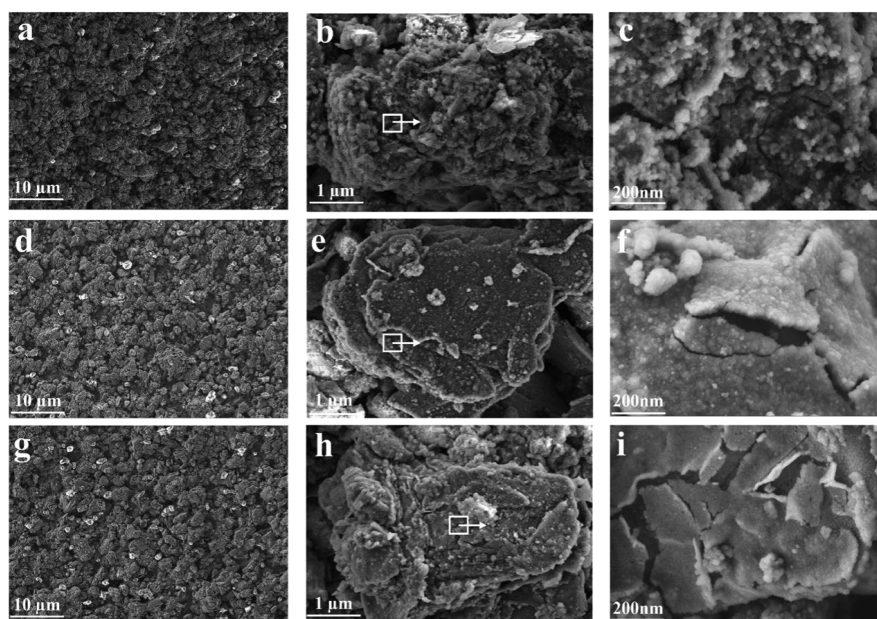
Figure 5. SEM images of different binders after 300 cycles under 0.2 A g^{-1}. (a–i) SiO$_x$/C anodes with PSAP663, PSA, and SA binders.

electrochemical tests was carried out on the SiO$_x$/C anodes with different binders. Figure 4a shows the cycling curves of SiO$_x$/C electrodes with different binders at low current density. In the first 10 cycles, the specific capacity of all the SiO$_x$/C electrodes showed a trend of rapid decline. This was mainly related to the formation of irreversible Li$_4$SiO$_4$ and the huge volume expansion, indicating that the commercial SiO$_x$/C materials had inherent instability. After that, all the SiO$_x$/C electrodes tended to been stable. On account of the carboxyl group having a more regular arrangement, it could form a strong bonding force with the surface of the SiO$_x$/C active material. At the same time, it could relieve the volume expansion of SiO$_x$/C particles and ensure the integrity of the electrode structure. Among these, the electrodes using PSAP as the binder exhibited better cycle stability that SA, indicating that addition of PAM and PTFE was an effective means to improve the electrochemical stability of the SiO$_x$/C. A comparison of the electrochemical performance of SiO$_x$/C anodes using PSAP binders with different ratios is shown in Figure 4a. After 250 cycles, the specific capacities of the anodes using PSAP447 and PSAP2211 were 461 and 441 mA h g^{-1}, respectively, which were lower than that of PSAP663 (498 mA h g^{-1}). This was mainly because the PSAP447 and PSAP2211 with a higher PTFE content (7 and 11% respectively) had a weaker bonding strength than PSAP663.

Figure S2a shows the cyclic voltammetry (CV) test of the SiO$_x$/C anode with PSAP663. Obviously, the first cathodic peak appeared at 0.797 V during the first cycle and then disappeared, mainly due to the formation of the SEI layer. The new cathode peak appearing in the back cycle was instead transformed from crystalline Si to amorphous Li$_4$SiO$_4$. The multiple anodic peaks at 0.25 and 0.285 V can be attributed to the delithiation reaction of the amorphous Li$_4$SiO$_4$ alloy and the formation of amorphous Si. Then, the cathode and anode peaks gradually increased with the increase of cycling times, indicating that Si was gradually active during lithium insertion/delithiation.

Figure S2b–d shows the charge/discharge curves of the SiO$_x$/C anodes with PSAP663, PSA, and SA at cycle 1, cycle

50, cycle 100, cycle 150, cycle 200, cycle 250, and cycle 300, respectively. In the first-cycle discharge curves of four different SiO$_x$/C electrodes, there was a long discharge platform between 0.01 and 0.08 V, reflecting the conversion process of crystal Si to amorphous Li$_4$SiO$_4$. In the charging platform, crystal Si was formed due to the dealloying process of the Li$_4$SiO$_4$ phase. In the first cycle and the 50th cycle, the charge capacities of four different binders SiO$_x$/C anodes were greatly reduced, which is the reason for the first 10 cycles in Figure 4a. During 50–250 cycles, the charge curves almost coincided, indicating that the delithiation process of SiO$_x$/C electrode material remained stable. It shows that the repeated expansion force of Si was effectively limited by the composite binder. After 250 cycles, PSAP633 remained stable, reflecting its good electrochemical performance.

Figure 4b shows the rate performance of the SiO$_x$/C anodes with different binders. The PSAP663 electrode shows the highest capacity, which can be ascribed to the fact that its good bonding ability can reduce the shedding of SiO$_x$/C particles. Besides, the amount of electrolyte absorbed should be paid attention. It is worth noting that PTFE was not added into PSA and SA so that the amount of the electrolyte absorbed by them was not sufficient, which had a negative impact on the capacity of the SiO$_x$/C. When the current increased to 1.2 A g^{-1}, the specific capacity of the PSAP663 (238 mA h g^{-1}) electrode was significantly higher than that of SA (102 mA h g^{-1}) and PSA (178 mA h g^{-1}). When the current returned to 0.1 A g^{-1}, the specific capacity of the four different electrodes could be restored to a great extent. Figure 4c shows the discharge cycle curve of the SiO$_x$/C anodes with different binders at 0.5 A g^{-1}. After 300 cycles, the specific capacity of the SiO$_x$/C anode with PSAP663 was 427 mA h g^{-1}. The specific capacity of the SiO$_x$/C anodes with PSA and SA decreased from the initial 592 and 491 to 200 and 210 mA h g^{-1}, respectively. The functional groups in SA like a gripper could keep the SiO$_x$ particles in their original position and make stable contact with graphite or conductive carbon. With the decrease of the SA content, the cycle stability of electrode
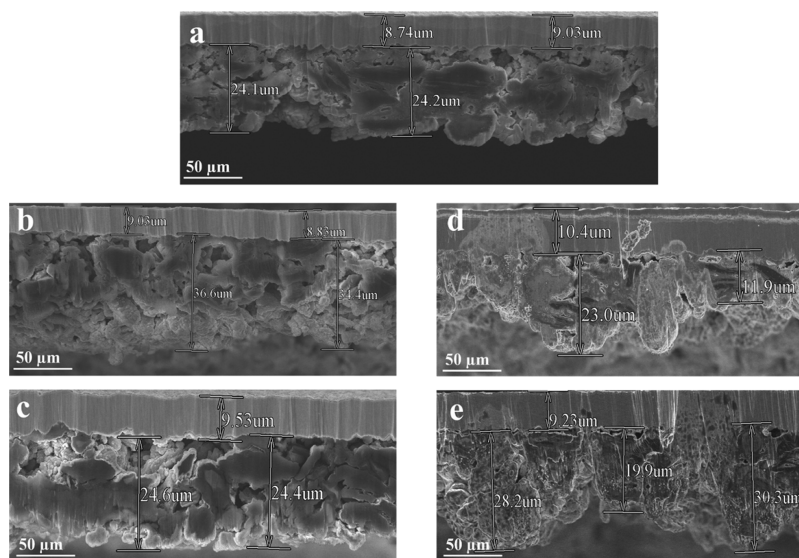
Figure 6. SEM images for the cutting section of the SiO$_x$/C anodes with different binders. (a−e) Corresponding to the cross-sectional ratio of PSAP663, PSAP447, PSAP2211, PSA, and SA after 300 cycles of discharge, the thickness of about 9 μm above the material is the cross-sectional size of the copper collector.

became worse. This also proves the correctness of allowing SA to account for the high ratio.

2.4. Analysis of the Working Mechanism of the Binder in the SiO$_x$/C Anode. In order to study the reasons for the different electrochemical performances of SiO$_x$/C anodes using different binders, the working mechanism was deeply analyzed. After 300 cycles at 0.2 A g^{-1}, the SEM images of the SiO$_x$/C electrodes using different binders (PSAP663, PSA, and SA) are shown in Figure 5a−i. By comparing the SEM images of each binder surface, it can be seen that the PSAP663 electrode surface in Figure 5a remains intact. In addition a large number of bright white particles were bonded around the SiO$_x$/C particles (Figure 5b,c), indicating that the PSAP663 binder had good stability in a long cycle. The PSA and SA electrodes show obvious uneven pits, indicating that the binders were peeled off seriously (Figure 5d−i). The SEM images of PSAP447, PSAP2211, and PSAP663 electrodes are shown in Figure S3a−d. After 300 cycles, some small pits can be found on the electrode surface with PSAP2211 and PSAP447, indicating that the SiO$_x$/C particles were peeled off from the electrodes.

In order to demonstrate the excellent effect of PSAP663 on the SiO$_x$/C anode, compared SiO$_x$/C electrodes with different binders before and after cycling. The images of the cross section of the SiO$_x$/C anodes with different binders before the cycling are shown in Figure S4a−e. After 300 cycles (Figure 6a), PSAP663 shows a strong superiority both in terms of the cross-sectional growth rate and contact with the Cu collector. It shows that the synergistic effect of rigid PAM and regular bonding forces in SA limits the expansion of SiO$_x$/C particles together, and the appropriate amount of the PTFE network coating effect leads to a complementary effect. For the PSAP447 material (Figure 6b), although the change in the cross section after 300 cycles was very small (about 36.4 μm), the PSAP outside the particle began to peel off the material surface gradually. This indicated that excessive absorption electrolyte caused by high PTFE content would cause massive side effects, which was not conducive to the stable operation of the battery. However, the overall surface structure remained

intact, so the specific capacity attenuation range was small in the long cycle performance diagram. After 300 cycles, the size of the cross sections of PSAP663 and PSAP2211 electrodes (about 24.2 μm) was the smallest among all the binders. Even though the volume of PSAP2211 after the cycling process (Figure 6c) did not change much, the contact between the active material and the Cu collector became smaller. Although the surface binder was still firmly bound to the surface of the material, because the amount of PAM and SA added was too small, the internal protection of the material was reduced. The contact with the Cu collector was less, and the conductivity was reduced, which naturally affected the performance of the battery under the long cycle. As for the cross-sectional changes of PSA and SA (Figure 6d,f), large areas of the coating binder of the two-electrode materials fell off before and after the cycling process. The bulk SiO$_x$/C material also began to expand greatly, resulting in uneven pits on the surface of the material. This is one of the main reasons for the specific capacity decay of the two materials after 300 cycles.

Based on the above results and analysis, Figure 7 shows the structural evolution diagram of the limiting effect of different components of the binder on SiO$_x$/C particles, highlighting the
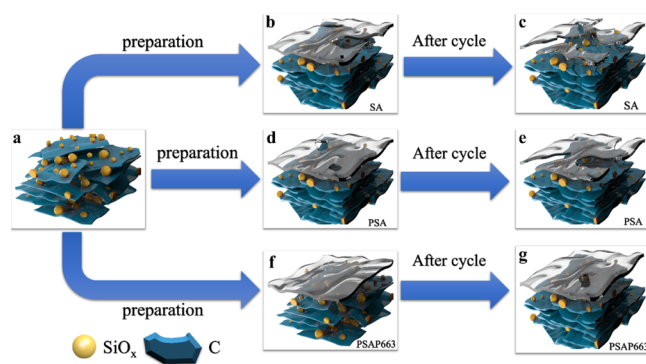
Figure 7. (a−g) Evolution of the SiO$_x$/C particles in the SiO$_x$/C anodes with SA, PSA, and PSAP663 binders over a long cycle and the action of the binders.

excellent electrochemical performance of PSAP663. In Figure 7a−f, it is obvious that PSAP663, PSA, and SA binder were uniformly coated on the surface of SiO_x/C particles before the battery cycle begun. In the initial stage, SiO_x/C particles were uniformly dispersed on the surface of the flaky graphite (Figure 7a). After preparing the electrode plates with different binders, it could be seen that the outer-coating binder of SiO_x/C, PSA, and SA-coated electrode all had more or less defects (Figure 7b,d). Instead, PAP663 was homogeneous and dense (Figure 7f). After 300 cycles, the binder around the SiO_x/C particles containing SA in Figure 7c fell off a lot, the volume of the central block SiO_x/C particles was much larger than that before the cycle, and many huge cracks appeared on the surface of the particles. The results indicated that a single SA binder could not maintain the repeated expansion of SiO_x/C particles for a long time, which led to the SA being peeled off. Although the binder shedding of SiO_x/C particles containing PSA (Figure 7e) was not very serious, it can be clearly seen that the volume of SiO_x/C changes greatly and the bonding force formed outside gradually loses its protective effect. This shows that the rigid force of PAM and the bond force of the SA law can limit the volume expansion of SiO_x/C in a long period of time. The capacity loss of the battery was serious due to excessive absorption of the electrolyte and excessive generation of the lithium salt in an irreversible reaction. For PSAP663 (Figure 7g), due to the introduction of PTFE, the amount of the electrolyte absorbed by the SiO_x/C electrode was appropriate, and the network structure of PTFE can match the defect of insufficient rigidity of PAM. It can limit the huge physical stress caused by the repeated expansion of SiO_x/C particles in the long cycle. After cycling, the bulk SiO_x/C particle volume did not change, the bond force formed on the surface acted on the SiO_x/C particle regularly and densely, and the PSAP coated on the surface was very compact and bonded around the SiO_x/C particle. Therefore, the SiO_x/C anode with PSAP663 shows excellent electrochemical performance.

3. CONCLUSIONS

In order to solve the problem of excessive attenuation of battery performance due to the repeated expansion of SiO_x/C particles, the multifunctional binders of water systems were used to prepare SiO_x/C electrodes. The SiO_x/C electrode using PSAP663 showed good performance both in terms of electrochemical performance and physical mechanical stress. The intermolecular interaction between alginate anions and SiO_x is the core element for the electrochemical stability of SiO_x. Like a gripper, it can keep the SiO_x particles in their original position and make stable contact with graphite or conductive carbon, which ensures the electronic path. The PAM contains abundant amide functional groups, which not only improves the strain resistance of the coating layer but also improves the affinity between SiO_x and other components. The PTFE can form an elastic network in the electrode matrix, and its strong electrolyte absorption capacity can ensure the transmission channel of lithium ions. Therefore, based on the good lithium ion and electron transmission channels, the SiO_x/C anode with PSAP663 shows excellent practical application prospects. At the same time, it can achieve the dual purpose of environmental protection and low cost, which can provide a reference for alleviating the expansion of Si-based materials.

4. EXPERIMENTAL SECTION

4.1. Preparation of the SiO$_x$/C Anodes. The SiO_x/C plates were prepared using a coating method typically used in the manufacturing factory of LIBs. The raw materials including PAM (M.W. 10,000), carbon nanotubes (CNTs), PTFE (50% aqueous solution), and SiO_x/C composite were obtained from Great Power Energy & Technology Co., Ltd. (Guangzhou, China) and Tinci Advanced Materials Co., Ltd. (Guangzhou, China). SA (M.W. 400,000) was purchased from Aladdin. The active slurry consisted of SiO_x/C, CNT, and binders at a weight ratio of 13:4:3. Taking the preparation of the SiO_x/C anode with a binder composition as an example, the PAM, SA, and PTFE mixed by 6, 6, and 3% of the total active slurry mass, respectively, were marked PSAP663. Similarly, 4, 4, and 7% and 2, 2, and 11% of the total active slurry mass were marked as PSAP447 and PSAP2211, respectively. The conductive additive CNTs were added into the above mixtures after 6 h of vigorous magnetic stirring treatment. Then, after another 6 h of stirring, SiO_x/C was added, and the mixture was subjected to an additional 8 h of stirring. The slurries obtained were spread onto a copper foil with a doctor blade and then dried under vacuum at 120 °C for 10 h. The calculated mass loading of SiO_x/C was 0.6−1.0 mg cm^{-2}. Similarly, for the preparation of PSA and SA active slurry, only the dry weight of different water binders was needed to be weighed. Then, it was prepared according to PSAP663. SiO_x/C electrode materials with different binders were obtained.

4.2. Electrochemical Measurements. 2032 coin-type half-cells with different binder SiO_x/C anode materials were assembled in a glovebox filled with argon, where the concentrations of water and oxygen were both lower than 0.1 ppm (Microna, Universal 2440/750/900, China). The SiO_x/C pole piece was a disc with a diameter of 12 mm cut from the SiO_x/C electrode pole piece prepared by the abovementioned traditional process. The counter electrode was pure lithium metal foil. The polypropylene film (Celgard 2400) was selected as the diaphragm, and 1 M $LiPF_6$ ethylene carbonate/dimethyl carbonate (EC/DEC/EMC = 1/1/1 volume ratio) and 5 wt % fluoroethylene carbonate was selected as the electrolyte. The constant current charge and discharge test and rate performance were carried out in the voltage range of 0.01−1.5 V through a computer-controlled battery test system (Neware, China). Both CV and electrochemical impedance spectroscopy (EIS) were performed on a CHI 660B electrochemical workstation (Chenhua, China).

4.3. Analysis and Characterization. A series of electrochemical tests was carried out for different water-based binders by preparing half-cells to ensure the electrochemical performances of the materials. Rate performance, constant current charge and discharge test, EIS, and CV were carried out on the battery test system and the CHI 660B electrochemical workstation. The frequency range was 0.1 Hz to 100 kHz, and the voltage range was 0.01−2.0 V. The CV scanning speed was 0.1 mV s^{-1}. The morphologies were characterized by scanning electron microscopy (SEM; FEI Quanta 250 FEG). A Nicolet 6700 (Thermo Nicolet Corporation) device was used to perform FTIR spectroscopy measurements. A Bruker D8 ADVANCE X-ray diffractometer ($K\alpha$ Cu, α = 1.54056 Å) was used to determine the X-ray diffraction patterns. The peeling test was conducted by an HY-0580 device (Hengyi Testing Instruments, Shanghai, China) to measure the adhesive strength of the binders. A cross-sectional laser cutting

instrument (Guangzhou Tianci) was used to analyze the bonding degree of the adhesive with the Cu current collector after charging and discharging. The electrolyte absorption capacity of the binder was indicated by the swellability of the electrode. The specific test method was to immerse the dry electrode in the electrolyte for 12 h to calculate the absorption of the electrolyte. The mass of the electrode before soaking was recorded as W_1, and the mass of the electrode piece after soaking and removing excess electrolyte from the surface was recorded as W_2. The swelling (S) calculation formula is $S = (W_2 - W_1)/W_1 \times 100\%$.[39]

4.4. Computational Methods. Ab initio molecular dynamics calculation was performed by the CP2K/Quickstep code.[40,41] CP2K/Quickstep employs a hybrid Gaussian and plane-wave basis set.[42] Generalized gradient functional PBE and Goedecker,[43] Teter, and Hutter (GTH)[44] pseudopotentials in conjunction with double-zeta polarized basis sets (DZVP) were used.[45] The plane-wave basis set was extended to a density cutoff of 350 Ry. The model had been equilibrated for about 6 ps, the simulation step was 1 fs, and the simulation temperature was 300 K. The supercell parameters were as follows: $a = b = 1.5360$ nm, $c = 1.9073$ nm, and $\alpha = \beta = \gamma = 90°$. The Si(0 0 1) surface was modeled as slabs, which consist of four atomic layers and were separated by a 20 Å vacuum region in order to avoid the interaction between the adjacent images. The bottom two layers of Si atoms were fixed to simulate the situation of the inner layer of atoms. The alginate anion was placed on the Si(0 0 1) surface, and there was no bond between them in the initial configuration.

ASSOCIATED CONTENT

Supporting Information

The Supporting Information is available free of charge at https://pubs.acs.org/doi/10.1021/acsomega.1c04544.

Important parameters of the multicomponent binders, electrochemical tests, and the SEM characterizations of the SiO$_x$/C anodes with different binders (PDF)

AUTHOR INFORMATION

Corresponding Authors

Zhen Ma − School of Chemistry, South China Normal University, Guangzhou 510006, PR China; Email: 20200124@m.scnu.edu.cn

Junmin Nan − School of Chemistry, South China Normal University, Guangzhou 510006, PR China; orcid.org/0000-0001-6862-8978; Email: jmnan@scnu.edu.cn

Authors

Haoyuan Liu − School of Chemistry, South China Normal University, Guangzhou 510006, PR China

Encheng Huangzhang − School of Chemistry, South China Normal University, Guangzhou 510006, PR China

Chenhao Sun − School of Chemistry, South China Normal University, Guangzhou 510006, PR China

Yanchao Fan − School of Chemistry, South China Normal University, Guangzhou 510006, PR China

Xiaoyang Zhao − Department of Environmental Engineering, Henan Polytechnic Institute, Nanyang 473009, PR China

Complete contact information is available at:
https://pubs.acs.org/10.1021/acsomega.1c04544

Notes
The authors declare no competing financial interest.

REFERENCES

(1) Zhou, G.; Li, F.; Cheng, H.-M. Progress in Flexible Lithium Batteries and Future Prospects. *Energy Environ. Sci.* **2014**, *7*, 1307−1338.

(2) Li, G.; Ouyang, T.; Xiong, T.; Jiang, Z.; Adekoya, D.; Wu, Y.; Huang, Y.; Balogun, M.-S. All-Carbon-Frameworks Enabled Thick Electrode with Exceptional High-Areal-Capacity for Li-Ion Storage. *Carbon* **2021**, *174*, 1−9.

(3) Huang, Y.; Yang, H.; Xiong, T.; Adekoya, D.; Qiu, W.; Wang, Z.; Zhang, S.; Balogun, M.-S. Adsorption Energy Engineering of Nickel Oxide Hybrid Nanosheets for High Areal Capacity Flexible Lithium-Ion Batteries. *Energy Storage Mater.* **2020**, *25*, 41−51.

(4) Zhou, S.; Huang, P.; Xiong, T.; Yang, F.; Yang, H.; Huang, Y.; Li, D.; Deng, J.; Balogun, M. S. Sub-Thick Electrodes with Enhanced Transport Kinetics via In Situ Epitaxial Heterogeneous Interfaces for High Areal-Capacity Lithium Ion Batteries. *Small* **2021**, *17*, 2100778.

(5) Yao, Z.; Xia, X.; Xie, D.; Wang, Y.; Zhou, C.-A.; Liu, S.; Deng, S.; Wang, X.; Tu, J. Enhancing Ultrafast Lithium Ion Storage of Li$_4$Ti$_5$O$_{12}$ by Tailored TiC/C Core/Shell Skeleton Plus Nitrogen Doping. *Adv. Funct. Mater.* **2018**, *28*, 1802756.

(6) Wang, H.; Cui, Y. Nanodiamonds for energy. *Carbon Energy* **2019**, *1*, 13−18.

(7) Yao, Z.; Yin, H.; Zhou, L.; Pan, G.; Wang, Y.; Xia, X.; Wu, J.; Wang, X.; Tu, J. Ti^{3+} Self-Doped Li$_4$Ti$_5$O$_{12}$ Anchored on N-Doped Carbon Nanofiber Arrays for Ultrafast Lithium-Ion Storage. *Small* **2019**, *15*, No. e1905296.

(8) Zhang, M.; Zhang, T.; Ma, Y.; Chen, Y. Latest Development of Nanostructured Si/C Materials for Lithium Anode Studies and Applications. *Energy Storage Mater.* **2016**, *4*, 1−14.

(9) Su, M.; Wan, H.; Liu, Y.; Xiao, W.; Dou, A.; Wang, Z.; Guo, H. Multi-Layered Carbon Coated Si-Based Composite as Anode for Lithium-Ion Batteries. *Powder Technol.* **2018**, *323*, 294−300.

(10) Chen, T.; Wu, J.; Zhang, Q.; Su, X. Recent Advancement of SiO$_x$ Based Anodes for Lithium-Ion Batteries. *J. Power Sources* **2017**, *363*, 126−144.

(11) Li, P.; Zhao, G.; Zheng, X.; Xu, X.; Yao, C.; Sun, W.; Dou, S. X. Recent Progress on Silicon-Based Anode Materials for Practical Lithium-Ion Battery Applications. *Energy Storage Mater.* **2018**, *15*, 422−446.

(12) Li, J.-Y.; Xu, Q.; Li, G.; Yin, Y.-X.; Wan, L.-J.; Guo, Y.-G. Research Progress Regarding Si-Based Anode Materials Towards Practical Application in High Energy Density Li-Ion Batteries. *Mater. Chem. Front.* **2017**, *1*, 1691−1708.

(13) Kasavajjula, U.; Wang, C.; Appleby, A. J. Nano- and Bulk-Silicon-Based Insertion Anodes for Lithium-Ion Secondary Cells. *J. Power Sources* **2007**, *163*, 1003−1039.

(14) Wu, H.; Chan, G.; Choi, J. W.; Ryu, I.; Yao, Y.; McDowell, M. T.; Lee, S. W.; Jackson, A.; Yang, Y.; Hu, L.; Cui, Y. Stable Cycling of Double-Walled Silicon Nanotube Battery Anodes through Solid-Electrolyte Interphase Control. *Nat. Nanotechnol.* **2012**, *7*, 310−315.

(15) Yang, J.; Wang, Y.-X.; Chou, S.-L.; Zhang, R.; Xu, Y.; Fan, J.; Zhang, W.-X.; Kun Liu, H.; Zhao, D.; Xue Dou, S. Yolk-Shell Silicon-Mesoporous Carbon Anode with Compact Solid Electrolyte Interphase Film for Superior Lithium-Ion Batteries. *Nano Energy* **2015**, *18*, 133−142.

(16) Zhou, X.; Yin, Y.-X.; Wan, L.-J.; Guo, Y.-G. Facile Synthesis of Silicon Nanoparticles Inserted into Graphene Sheets as Improved Anode Materials for Lithium-Ion Batteries. *Chem. Commun.* **2012**, *48*, 2198−2200.

(17) Jin, Y.; Kneusels, N.-J. H.; Marbella, L. E.; Castillo-Martínez, E.; Magusin, P. C. M. M.; Weatherup, R. S.; Jónsson, E.; Liu, T.; Paul, S.;

Grey, C. P. Understanding Fluoroethylene Carbonate and Vinylene Carbonate Based Electrolytes for Si Anodes in Lithium Ion Batteries with NMR Spectroscopy. *J. Am. Chem. Soc.* **2018**, *140*, 9854−9867.

(18) Zhao, Y.; Yang, L.; Zuo, Y.; Song, Z.; Liu, F.; Li, K.; Pan, F. Conductive Binder for Si Anode with Boosted Charge Transfer Capability via n-Type Doping. *ACS Appl. Mater. Interfaces* **2018**, *10*, 27795−27800.

(19) Lee, S. H.; Lee, J. H.; Nam, D. H.; Cho, M.; Kim, J.; Chanthad, C.; Lee, Y. Epoxidized Natural Rubber/Chitosan Network Binder for Silicon Anode in Lithium-Ion Battery. *ACS Appl. Mater. Interfaces* **2018**, *10*, 16449−16457.

(20) Zhang, Z.; Jiang, Y.; Peng, Z.; Yang, S.; Lin, H.; Liu, M.; Wang, D. Facile Pyrolyzed N-Doped Binder Network for Stable Si Anodes. *ACS Appl. Mater. Interfaces* **2017**, *9*, 32775−32781.

(21) Roy, A. K.; Zhong, M.; Schwab, M. G.; Binder, A.; Venkataraman, S. S.; Tomović, Ž. Preparation of a Binder-Free Three-Dimensional Carbon Foam/Silicon Composite as Potential Material for Lithium Ion Battery Anodes. *ACS Appl. Mater. Interfaces* **2016**, *8*, 7343−7348.

(22) Hu, S.; Cai, Z.; Huang, T.; Zhang, H.; Yu, A. A Modified Natural Polysaccharide as a High-Performance Binder for Silicon Anodes in Lithium-Ion Batteries. *ACS Appl. Mater. Interfaces* **2019**, *11*, 4311−4317.

(23) Yang, Y.; Wu, S.; Zhang, Y.; Liu, C.; Wei, X.; Luo, D.; Lin, Z. Towards Efficient Binders for Silicon Based Lithium-Ion Battery Anodes. *Chem. Eng. J.* **2021**, *406*, 126807.

(24) Li, J.; Zhang, G.; Yang, Y.; Yao, D.; Lei, Z.; Li, S.; Deng, Y.; Wang, C. Glycinamide Modified Polyacrylic Acid as High-Performance Binder for Silicon Anodes in Lithium-Ion Batteries. *J. Power Sources* **2018**, *406*, 102−109.

(25) Hu, Y.-Y.; You, J.-H.; Zhang, S.-J.; Lin, H.; Ren, W.-F.; Deng, L.; Pan, S.-Y.; Huang, L.; Zhou, Y.; Li, J.-T.; Sun, S.-G. Li₀.₅PAA Domains Filled in Porous Sodium Alginate Skeleton: A 3D Bicontinuous Composite Network Binder to Stabilize Micro-Silicon Anode for High-performance Lithium Ion Battery. *Electrochim. Acta* **2021**, *386*, 138361.

(26) Kang, T.; Chen, J.; Cui, Y.; Wang, Z.; Xu, H.; Ma, Z.; Zuo, X.; Xiao, X.; Nan, J. Three-Dimensional Rigidity-Reinforced SiO_x Anodes with Stabilized Performance Using an Aqueous Multicomponent Binder Technology. *ACS Appl. Mater. Interfaces* **2019**, *11*, 26038−26046.

(27) Gendensuren, B.; Oh, E.-S. Dual-Crosslinked Network Binder of Alginate with Polyacrylamide for Silicon/Graphite Anodes of Lithium Ion Battery. *J. Power Sources* **2018**, *384*, 379−386.

(28) Li, R.; Bai, C.-J.; Liu, H.; Yang, L.-W.; Ming, Y.; Xu, C.-L.; Wei, Z.; Song, Y.; Wang, G.-K.; Liu, Y.-X.; Zhong, B.-H.; Zhong, Y.-J.; Wu, Z.-G.; Guo, X.-D. New Insights into the Mechanism of Enhanced Performance of $Li[Ni_{0.8}Co_{0.1}Mn_{0.1}]O_2$ with a Polyacrylic Acid-Modified Binder. *J. Power Sources* **2021**, *13*, 10064−10070.

(29) Hwang, J.-Y.; Myung, S.-T.; Sun, Y.-K. Sodium-Ion Batteries: Present and Future. *Chem. Soc. Rev.* **2017**, *46*, 3529−3614.

(30) Lim, S.; Chu, H.; Lee, K.; Yim, T.; Kim, Y.-J.; Mun, J.; Kim, T.-H. Physically Cross-linked Polymer Binder Induced by Reversible Acid-Base Interaction for High-Performance Silicon Composite Anodes. *ACS Appl. Mater. Interfaces* **2015**, *7*, 23545−23553.

(31) Eliseeva, S. N.; Kamenskii, M. A.; Tolstopyatova, E. G.; Kondratiev, V. V. Effect of Combined Conductive Polymer Binder on the Electrochemical Performance of Electrode Materials for Lithium-Ion Batteries. *Energies* **2020**, *13*, 2163.

(32) Li, S.; Zhu, M.; Liu, J.; Yu, M.; Wu, L.; Zhang, J.; Liang, H. Enhanced Tribological Behavior of Anodic Films Containing SiC and PTFE Nanoparticles on Ti_6Al_4V Alloy. *Appl. Surf. Sci.* **2014**, *316*, 28−35.

(33) Watanabe, T.; Hirai, K.; Ando, F.; Kurosumi, S.; Ugawa, S.; Lee, H.; Irii, Y.; Maki, F.; Gunji, T.; Wu, J.; Ohsaka, T.; Matsumoto, F. Surface Double Coating of a $LiNi_aCo_bAl_{1−a−b}O_2$ (a >0.85) Cathode with TiO_x and Li_2CO_3 to Apply a Water-Based Hybrid Polymer Binder to Li-Ion Batteries. *RSC Adv.* **2020**, *10*, 13642−13654.

(34) Miranda, A.; Li, X.; Haregewoin, A. M.; Sarang, K.; Lutkenhaus, J.; Kostecki, R.; Verduzco, R. A Comprehensive Study of Hydrolyzed Polyacrylamide as a Binder for Silicon Anodes. *ACS Appl. Mater. Interfaces* **2019**, *11*, 44090−44100.

(35) Zhu, X.; Zhang, F.; Zhang, L.; Zhang, L.; Song, Y.; Jiang, T.; Sayed, S.; Lu, C.; Wang, X.; Sun, J.; Liu, Z. A Highly Stretchable Cross-Linked Polyacrylamide Hydrogel as an Effective Binder for Silicon and Sulfur Electrodes toward Durable Lithium-Ion Storage. *Adv. Funct. Mater.* **2018**, *28*, 1705015.

(36) Hong, S. Y.; Kim, Y.; Park, Y.; Choi, A.; Choi, N.-S.; Lee, K. T. Charge Carriers in Rechargeable Batteries: Na Ions vs. Li Ions. *Energy Environ. Sci.* **2013**, *6*, 2067−2081.

(37) Ling, L.; Bai, Y.; Wang, Z.; Ni, Q.; Chen, G.; Zhou, Z.; Wu, C. Remarkable Effect of Sodium Alginate Aqueous Binder on Anatase TiO_2 as High-Performance Anode in Sodium Ion Batteries. *ACS Appl. Mater. Interfaces* **2018**, *10*, 5560−5568.

(38) Gauch, M.; Ehlers, H.; Ristau, D. Mixing of PTFE and Oxides by Sputtering Techniques: A Comparison of Different Approaches. *Procedia Technol.* **2014**, *15*, 540−548.

(39) Li, X.; Yan, P.; Xiao, X.; Woo, J. H.; Wang, C.; Liu, J.; Zhang, J.-G. Design of Porous Si/C−Graphite Electrodes with Long Cycle Stability and Controlled Swelling. *Energy Environ. Sci.* **2017**, *10*, 1427−1434.

(40) Hutter, J.; Iannuzzi, M.; Schiffmann, F.; VandeVondele, J. Cp2k: Atomistic Simulations of Condensed Matter Systems. *WIRES Comput. Mol. Sci.* **2014**, *4*, 15−25.

(41) VandeVondele, J.; Krack, M.; Mohamed, F.; Parrinello, M.; Chassaing, T.; Hutter, J. Quickstep: Fast and Accurate Density Functional Calculations Using a Mixed Gaussian and Plane Waves Approach. *Comput. Phys. Commun.* **2005**, *167*, 103−128.

(42) Lippert, G.; Hutter, J.; Parrinello, M. A hybrid Gaussian and plane wave density functional scheme. *Mol. Phys.* **1997**, *92*, 477−487.

(43) Perdew, J.; Burke, K.; Ernzerhof, M. Generalized Gradient Approximation Made Simple. *Phys. Rev. Lett.* **1996**, *77*, 3865−3868.

(44) Goedecker, S.; Teter, M.; Hutter, J. Separable Dual-space Gaussian Pseudopotentials. *Phys. Rev. B: Condens. Matter Mater. Phys.* **1996**, *54*, 1703−1710.

(45) VandeVondele, J.; Hutter, J. Gaussian Basis Sets for Accurate Calculations on Molecular Systems in Gas and Condensed Phases. *J. Chem. Phys.* **2007**, *127*, 114105.